WHOLE–CORE NEUTRON TRANSPORT CALCULATIONS WITHOUT FUEL-COOLANT HOMOGENIZATION

M. A. Smith, N. Tsoulfanidis
University of Missouri, Rolla
Department of Nuclear Engineering
Rolla, Missouri 65409

E. E. Lewis
Northwestern University
Department of Mechanical Engineering
Evanston, Illinois 60208

G. Palmiotti & T. A. Taiwo
Argonne National Laboratory
9700 South Cass Avenue
Argonne, Illinois 60439

ABSTRACT

The variational nodal method implemented in the VARIANT code is generalized to perform full core transport calculations without spatial homogenization of cross sections at either the fuel-pin cell or fuel assembly level. The node size is chosen to correspond to one fuel-pin cell in the radial plane. Each node is divided into triangular finite subelements, with the interior spatial flux distribution represented by piecewise linear trial functions. The step change in the cross sections at the fuel-coolant interface can thus be represented explicitly in global calculations while retaining the full spherical harmonics capability of VARIANT. The resulting method is applied to a two-dimensional seven-group representation of a LWR containing MOX fuel assemblies. Comparisons are made of the accuracy of various space-angle approximations and of the corresponding CPU times.

1. Introduction

Nodal methods have found widespread use for the performance of whole-core reactor physics calculations. Each node normally corresponds to an axial slice of a fuel assembly for which homogenized cross sections have first been obtained. The methods have been most widely applied using diffusion theory for two-group thermal reactor calculations but also to multigroup fast reactor calculations. In fast reactor cores, however, and with increasingly heterogeneous

thermal reactor cores, steep flux gradients and large cross section discontinuities may cause the diffusion approximation to lead to substantial inaccuracies.

Nodal transport theory is employed increasingly to circumvent diffusion theory's limitations. In particular, the variational nodal method incorporated into the Argonne National Laboratory code VARIANT combines multigroup spherical harmonics (Pn) or simplified spherical harmonics (SPn) treatments of the angular variables with a nodal treatment of the spatial variables based on a hybrid primal finite element method.[2-5, 8] VARIANT utilizes response matrix methods to solve the even-parity transport equation on a nodal grid coupled by odd-parity Lagrange multipliers at the node interfaces.

With the ability to perform whole-core nodal transport calculations secured, the largest remaining computational uncertainties arise from the use of homogenized fuel assembly cross sections and the subsequent dehomogenization procedures required to estimate fuel pin powers. For, no matter how high the angular order of whole-core transport calculations, accuracy is limited by the approximations made in the homogenization process. In highly heterogeneous configurations, such as those in LWRs containing MOX fuel assemblies, the spatial homogenization performed at the fuel-pin cell or at the fuel assembly level may obliterate the coupling between local and global transport effects and introduce substantial errors into pin power estimates.

Our recent efforts have been centered on generalizing the variational nodal method to perform whole-core transport calculations in which the need for spatial cross section homogenization is reduced or eliminated. To accomplish this, we introduce a subelement formulation to expand the capabilities of the VARIANT code. The resulting algorithms are more computationally intensive than those employed with homogenized assembly cross sections. Nevertheless, continuing advances in processor speed and the improving capabilities for parallel computing make the prospects bright for employing such methods not only for occasional benchmark verifications but also for more routine reactor physics calculations as well.

The standard VARIANT code employs a set of complete polynomial trial functions to represent the flux within each homogenized node. More recently, we have developed two different approaches to refining the spatial resolution, both retaining full capability to perform Pn or SPn approximations in angle. In the first of these, the homogeneous assembly-sized nodes conventionally used in VARIANT are replaced with homogeneous nodes each the size of one fuel-pin cell. Full core calculations thus require homogenization only at the fuel-pin cells. The refined spatial resolution, however, considerably lengthens the time required to obtain a solution of the resulting response matrix equations. The second approach uses finite subelement trial functions.

With subelements, the fuel assembly is retained as the basic node. Within each node, continuous, piecewise bilinear finite subelement trial functions are employed on a square grid, corresponding to the pin cells. This approach permits step changes in cross sections at each pin cell interface. As in the first approach, homogenization is required only at fuel-pin cell level. Retaining the assembly-sized node incurs some approximation along the assembly interfaces that is not present in the first approach. However, our experience with two-group MOX loaded LWR

cores indicates that the errors introduced are quite small[5,6]. Moreover, retaining the large assembly-sized nodes results in faster solution of the response matrix equations while moving the additional computational effort to the highly parallelizable formation of the response matrices.

In the following section, we present a third approach that also uses subelements, but in a quite different manner. In it, the nodes are the size of one fuel-pin cell. Within each node, continuous piecewise linear finite element trial functions are utilized on a triangular grid. As indicated in Fig. 1 such grids allow the step change in cross sections at the fuel-coolant interfaces to be represented explicitly. Thus homogenization at both the fuel-pin cell and the fuel assembly levels is eliminated. In section 3 we apply this formulation to a seven-group MOX benchmark problem and examine accuracy and computational efficiency. Future directions are discussed in the final section.

2. Theory

The variational nodal method combines multigroup spherical harmonics (Pn) or simplified spherical harmonics (SPn) expansions of the angular variables with a primal hybrid finite element representation in space of the even-parity form of the transport equation. The problem domain V is decomposed into subdomains V_n (called nodes of elements):

$$V = \sum_n V_n . \tag{1}$$

The even-parity transport equation is solved within each node, with the nodes coupled by odd-parity Lagrange multipliers that preserve nodal neutron balance.

Following the angular expansion, the even-parity equations reduce to a coupled set of second order differential equations[6]

$$-\vec{\nabla}\cdot \boldsymbol{s}^{-1}\vec{\mathbf{E}}\vec{\mathbf{E}}^T\cdot\vec{\nabla}\mathbf{y}^+(\vec{r})+\boldsymbol{s}\mathbf{y}^+(\vec{r})=\boldsymbol{s}_s\mathbf{w}\mathbf{w}^T\mathbf{y}^+(\vec{r})+\mathbf{s}(\vec{r}), \quad \vec{r}\in V_n \tag{2}$$

where $\mathbf{y}^+(\vec{r})$ is the vector of spatially dependent coefficients of the even-parity flux, and the angular coupling is incorporated into the tensor $\vec{\mathbf{E}}$ and the vector w. The odd-parity coefficient vector on the node interfaces is given by

$$\mathbf{y}^-(\vec{r})=-\boldsymbol{s}^{-1}\vec{\nabla}\cdot\vec{\mathbf{E}}^T\mathbf{y}^+(\vec{r}). \qquad \vec{r}\in\Gamma_n \tag{3}$$

To express these equations in a variational form, we define a functional that is a superposition of nodal contributions

$$F[\mathbf{y}^+,\mathbf{y}^-]=\sum_n F_n[\mathbf{y}^+,\mathbf{y}^-], \tag{4}$$

where

$$F_n[\mathbf{y}^+,\mathbf{y}^-]=\int_n dV\left\{\boldsymbol{\sigma}^{-1}(\vec{\nabla}\cdot\vec{\mathbf{E}}^T\mathbf{y}^+)^T(\vec{\nabla}\cdot\vec{\mathbf{E}}^T\mathbf{y}^+)+\mathbf{y}^{+T}(\boldsymbol{\sigma}\mathbf{I}-\sigma_s\mathbf{w}\mathbf{w}^T)\mathbf{y}^+-2\mathbf{y}^{+T}\mathbf{s}\right\}$$
$$+2\int_n d\Gamma\hat{n}\cdot(\vec{\mathbf{E}}^T\mathbf{y}^+)^T\mathbf{y}^- . \qquad (5)$$

The functional is required to be stationary, yielding Eq. (2) as the Euler-Lagrange equation resulting from variations in $\mathbf{y}^+(\vec{r})$ within the node, and Eq. (3) at the interfaces. Similarly, continuity of $\mathbf{y}^+(\vec{r})$ across the nodal interfaces is imposed from variations on the interface Lagrange multipliers $\mathbf{y}^-(\vec{r})$.

We next discretize the spatial variables. The interface Lagrange multiplier vectors are expanded as

$$\mathbf{y}^-(\vec{r})=\mathbf{I}_N\otimes\mathbf{h}^T(\vec{r})\mathbf{c}_n, \qquad \vec{r}\in\Gamma_n \qquad (6)$$

where the J spatial trial functions $\mathbf{h}(\vec{r})$ obey the orthogonality condition

$$\int_n d\Gamma\mathbf{h}\mathbf{h}^T=\mathbf{I}_J . \qquad (7)$$

and $\otimes$ indicates Kronecker tensor multiplication.

In the standard form of VARIANT, the cross sections within each node are uniform and $\mathbf{y}^+(\vec{r})$ is expanded in a set of complete polynomials, typically of fourth or sixth order. Here, however, we want to treat fuel-pin cells as heterogeneous nodes in which the fuel-coolant interface is represented explicitly. To accomplish this we subdivide the nodal volume V_n into a number of triangular subelements.

$$V_n=\sum_e V_e . \qquad (8)$$

where uniform cross sections are specified within each subelement. In the calculations that follow, the triangular element structures indicated in Fig. 1 are used to represent explicitly the fuel-coolant interface in a unit cell sized node. They are specified such that the fuel and coolant volume fractions are preserved exactly.

We represent spatial flux distributions within each subelement by finite element trial functions with local support, designated by the vector $\mathbf{n}(\vec{r})$, and vectors $\mathbf{x}_e$ of unknowns. The even-parity flux moments become

$$\mathbf{y}^+(\vec{r})=\mathbf{I}_M\otimes\mathbf{n}^T(\vec{r})\mathbf{x}_e, \qquad \vec{r}\in V_e \qquad (9)$$

where $\mathbf{n}(\vec{r})$ represents the linear trial functions on the triangular elements. Hence $\mathbf{x}_e$ approximates the value of $\mathbf{y}^+(\vec{r})$ at the subelement vertices. The nodal functional given by Eq.(12) reduces to a superposition of subelement contributions:

$$F_n[\mathbf{z}_n, \mathbf{c}_n] = \sum_e \mathbf{x}_e^T \mathbf{A}_e \mathbf{x}_e - 2\sum_e \mathbf{x}_e^T \mathbf{s}_e + 2\sum_e \mathbf{x}_e^T \mathbf{M}_e \mathbf{c}_n, \tag{10}$$

where the coefficient matrices are given in terms of the known trial functions

$$\mathbf{A}_e = \boldsymbol{\sigma}_e^{-1} \mathbf{E}_k \mathbf{E}_{k'}^T \otimes \int_e dV (\nabla_k \mathbf{n})(\nabla_{k'} \mathbf{n}^T) + (\boldsymbol{\sigma}_e \mathbf{I} - \boldsymbol{\sigma}_{se} \mathbf{w}\mathbf{w}^T) \otimes \int_e dV \mathbf{n}\mathbf{n}^T, \tag{11}$$

and

$$\mathbf{M}_e = \mathbf{E}_k \otimes \int_e d\Gamma n_k \mathbf{n}\mathbf{h}^T, \tag{12}$$

with the source term

$$\mathbf{s}_e = \int_e dV \mathbf{s} \otimes \mathbf{n}. \tag{13}$$

Since these trial functions must be continuous across subelement interfaces, the components of $\mathbf{x}_e$ corresponding to the same physical location on either side of a subelement interface must have the same value. This continuity condition is enforced by creating a Boolean matrix $\mathbf{X}_e$ for each subelement that maps the $\mathbf{x}_e$ onto $\mathbf{z}_n$, a node wide vector of coefficients:

$$\mathbf{x}_e = \mathbf{X}_e \mathbf{z}_n. \tag{14}$$

Assembling the subelements, we may write the discretized forms of Eqs. (4) and (5) as

$$F = \sum_n F_n[\mathbf{z}_n, \mathbf{c}_n] \tag{15}$$

and

$$F_n[\mathbf{z}_n, \mathbf{c}_n] = \mathbf{z}_n^T \mathbf{A}_n \mathbf{z}_n - 2\mathbf{z}_n^T \mathbf{s}_n + 2\mathbf{z}_n^T \mathbf{M}_n \mathbf{c}_n \tag{16}$$

where $\mathbf{A}_n = \sum_e \mathbf{X}_e^T \mathbf{A}_e \mathbf{X}_e$, $\mathbf{M}_n = \sum_e \mathbf{X}_e^T \mathbf{M}_e$ and $\mathbf{s}_n = \sum_e \mathbf{X}_e^T \mathbf{s}_e$.

To speed computations without a commensurate loss of accuracy, the group source vector can be lumped into coarser components. They are the volume-averaged contributions from the fuel and

from the moderator regions adjoining the four cell interfaces, as indicated by the shading in Fig.1.

Requiring Eq. (16) to be stationary with respect to variations in $\mathbf{z}_n$ and $\mathbf{c}_n$ yields for each node, the equation

$$\mathbf{A}_n \mathbf{z}_n + \mathbf{M}_n \mathbf{c}_n = \mathbf{s}_n \tag{17}$$

and the continuity of

$$\mathbf{y}_n = \mathbf{M}_n^T \mathbf{z}_n \tag{18}$$

across each interface. Solving Eq. (17) for $\mathbf{z}_n$ yields

$$\mathbf{z}_n = \mathbf{A}_n^{-1}\mathbf{s}_n - \mathbf{A}_n^{-1}\mathbf{M}_n \mathbf{c}_n . \tag{19}$$

The combination of Eq. (18) and (19) then gives the result

$$\mathbf{y}_n = \mathbf{M}_n^T \mathbf{A}_n^{-1}\mathbf{s}_n - \mathbf{M}_n^T \mathbf{A}_n^{-1}\mathbf{M}_n \mathbf{c}_n . \tag{20}$$

This equation expresses the even-parity flux moments $\mathbf{y}_n$ at the node interface in terms of the source and the odd-parity interface moments $\mathbf{c}_n$, while imposing the continuity of both of these moments between neighboring elements. The final step is to transform variables such that Eq.(20) may be written in terms of a response matrix. Introducing the partial current like variables

$$\mathbf{j}_n^{\pm} = \tfrac{1}{4}\mathbf{y}_n \pm \tfrac{1}{2}\mathbf{c}_n , \tag{21}$$

we may write Eq.(20) in the response matrix form:

$$\mathbf{j}_n^{+} = \mathbf{R}_n \mathbf{j}_n^{-} + \mathbf{B}_n \mathbf{s}_n . \tag{22}$$

3. Results

The finite subelement formulation described above has been implemented in a prototypic modification of the VARIANT code. We have applied it to a problem being proposed as an OECD/NEA benchmark.[7] The problem is an elaboration of the earlier OECD/NEA two group PWR benchmark, C5 configuration.[1] The quarter core configuration, shown in Fig. 2 consists of two MOX and two UO_2 assemblies. The configuration of the MOX assemblies is indicated in Fig. 3, where the shading indicates the three Plutonium enrichments, and the guide tubes. In the UO_2 assemblies all of the fuel pins have the same composition. The C5 configuration poses a

challenging transport problem since the heterogeneities produced by the MOX assembles interact strongly with the sharp global flux gradients that result from the small core size.

As a basis for the calculations that follow, we took the atom densities specified by Cavarec, 1994, and performed single fuel-pin cell calculations with the DRAGON code[9] to generate seven-group transport-corrected isotropic cross sections for the fuel and for the coolant regions of each fuel-pin cell. Our concern was not with the accuracy lost in cross section collapse, but rather with spatial homogenization and space-angle transport effects. Thus we simplified the resulting cross section set by using a single set of water cross sections (those from the UO_2 cell) for all the assemblies and for the reflector.

We performed two classes of calculations in which each node represents one fuel-pin cell. The first uses the subelement formulation of VARIANT where no spatial homogenization is employed either at the fuel-pin cell or fuel assembly level. The second uses the standard VARIANT formulation, which requires homogenized fuel-pin cell cross sections. The homogenized cross sections are generated using standard flux weighting from the single pin cell calculations. Comparing the results of standard and subelement VARIANT calculations thus allows inaccuracies produced by pin cell homogenization to be examined.

The subelement VARIANT formulation allows all of the space-angle approximations to be refined: node interface approximations from flat to linear to quadratic, triangular meshes from Fig. 1a to Fig. 1b, and angular approximations from P1, to P3, and P5. Multiple geometry comparisons were carried out between the higher-order approximations of both the standard and subelement VARIANT codes and the DRAGON collision probability code calculations using the seven group cross sections as input. For single-pin cell geometries, both the standard version of VARIANT and the subelement version are in excellent agreement with the eigenvalue results from DRAGON. The same is true for calculations of single fuel assembly geometries. For the C5 configuration a full collision probability calculation using the DRAGON code could not be completed because of excessive CPU time (longer than one month). Thus we only compare the differences between the standard version of VARIANT and the subelement version taking the highest order subelement version as the reference solution.

Table I is a compendium of some of the VARIANT subelement results for the eigenvalue and peak to average pin power ratios for the C5 problem. As indicated in Table I, we found that a change in node interface approximation from linear to quadratic did not have a large effect on either eigenvalue or on the peak to average pin power ratio. A similar trend was observed with the change from flat to linear, therefore only partial results are included. It is noteworthy, however, that the estimate of some of the pin powers away from the peak are sensitive to the node interface approximation used. In the C5 problem, refinement of the triangular grid from Fig 1a to Fig 1b results in slightly larger eigenvalues and more substantial differences in peak to average pin power ratios, indicating the need for the more refined grid. As expected, the change in the angular approximation from P1 (diffusion) to P3 to P5 represents the most significant change in eigenvalue and peak to average pin power ratio results. The greatest change is observed between the P1 and P3 results, with a small correction made by the P5 calculation. These results are consistent with previous calculations made with VARIANT. In Fig. 4 the pin power distribution for the case with no homogenization (Fig. 1b triangular mesh) and that with

fuel-pin cell homogenization are shown. These results represent the solutions using a quadratic node interface approximation and a P5 angular approximation for both methods.

For the highest node interface approximation and angular approximation the total CPU times required for a Sun Ultra Workstation to obtain the problem solutions are 1690, 1820, and 2100 seconds for the standard VARIANT, coarse grid subelement VARIANT (Fig. 1a), and fine grid subelement VARIANT (Fig. 1b) calculations, respectively. In the case of the Fig. 1a mesh and the standard VARIANT calculation the time required to form the response matrices is almost identical (~25 seconds) with the triangular mesh taking slightly longer. The CPU time for the formation of the response matrices for the Fig. 1b mesh is on average twice that of the Fig. 1a mesh (~50-60 seconds). This shows that the majority of CPU time is devoted to the solution of the response matrix equations, which is relatively unaffected by the refinement of the spatial distribution within the node.

4. Discussion

The results given above offer encouragement for the further development of whole-core transport methods that eliminate the ambiguities introduced by homogenization at the fuel-pin cell and fuel assembly level. Much remains to be done both in improving the computational efficiency of the subelement methods and in extending them to a wider range of physical models.

For computational efficiency, the use of fuel assembly-size nodes, but nodes in which a richer triangular finite element structure would allow the explicit treatment of the fuel coolant interfaces, would greatly decrease the execution times for the outer iterations. The computational burden would then be shifted to finite element formation of the assembly response matrices. Such response matrix formulations would be ideally suited for parallel processor configurations, which are coming into increased use.

The more immediate modeling challenge is to take the subelement methods from two to three dimensions. Nodal interfaces will be required in the axial plane and, unlike planes lying perpendicular to the core axis, material interfaces will cut through these axial interfaces.

Acknowledgements

This work was supported by the U.S. Department of Energy under Contract No. W-31-109-ENG-38 and by U.S. Department of Energy Contract No. DE-FG07-98ID13632.

References

1. Cavarec, C., et al., "The OECD/NEA Benchmark Calculations of Power Distributions within Assemblies," ElectricitJ de France, Sept. 1994.

2. Carrico, C. B., Palmiotti, G., Lewis, E. E., "Progress and Applications of the Variational Nodal Method," Proc. Int. Topl. Mtg. on Mathematics and Computation, Portland, OR, April, 1995.

3. Lewis, E. E., C. B. Carrico, Palmiotti, G., "Variational Nodal Formulation of the Spherical Harmonics Equations," Nucl. Sci. Eng. **122**, 194, 1996.

4. Lewis, E. E., Palmiotti, G., "Simplified Spherical Harmonics in the Variational Nodal Method," Nucl. Sci. Eng., **126**, 48, 1997.

5. Lewis, E. E., Palmiotti, G. & Taiwo, T. A., "Whole-Core Comparisons of Subelement and Fine-Mesh Variational Nodal Methods," Trans. Am. Nucl. Soc. **80,** 117, 1999.

6. Lewis, E. E., Palmiotti, G. & Taiwo, T. A., "Space-Angle Approximations in the Variational Nodal Method," Proc. Int. Conf. Mathematics and Computation, Reactor Physics and Environmental Analysis of Nuclear Systems, Madrid, 27-30 Sept. 1999

7. E. E. Lewis, G. Palmiotti, T. A. Taiwo, M. A. Smith, & N. Tsoulfanidis, Benchmark Proposed to the OECD/NEA Three-Dimensional Radiation Transport Committee, unpublished, Jan. 2000

8. Palmiotti, G., Lewis, E. E., Carrico, C. B., "VARIANT: VARIational Anisotropic Nodal Transport for Multidimensional Cartesian and Hexagonal Geometry Calculation," Argonne National Laboratory ANL-95/40, 1995.

9. G. Marleau et al., "A User's Guide for DRAGON, " Ecole Polytechnique de Montréal, December 1997.

TABLE I. Eigenvalue and Peak to Avg. Pin Power Ratios for the C5 Problem.

		Homogenized Pin Cell VARIANT		Coarse Mesh (Fig. 1a)		Fine Mesh (Fig. 1b)	
Interface Approx.	Angular Approx.	Eigenvalue	Peak to Avg.	Eigenvalue	Peak to Avg.	Eigenvalue	Peak to Avg.
Linear	P1	1.18647	2.51679	1.18405	2.50592	1.18288	2.51372
Quadratic	P1	1.18651	2.51729	1.18411	2.50468	1.18305	2.50862
Quadratic	P3	1.18794	2.52887	1.18971	2.55758	1.19043	2.54115
Quadratic	P5	1.18803	2.52534	1.19055	2.55617	1.19181	2.53504
Interface Approx.	Angular Approx.	Percent Diff	Percent Diff	Percent Diff	Percent Diff	Percent Diff	Percent Diff
Linear	P1	0.44746	0.72019	0.65088	1.14873	0.74867	0.84121
Quadratic	P1	0.44447	0.70035	0.64537	1.19767	0.73491	1.04226
Quadratic	P3	0.32441	0.24337	0.17617	0.88883	0.11522	0.24072
Quadratic	P5	0.31687	0.38291	0.10567	0.83328		

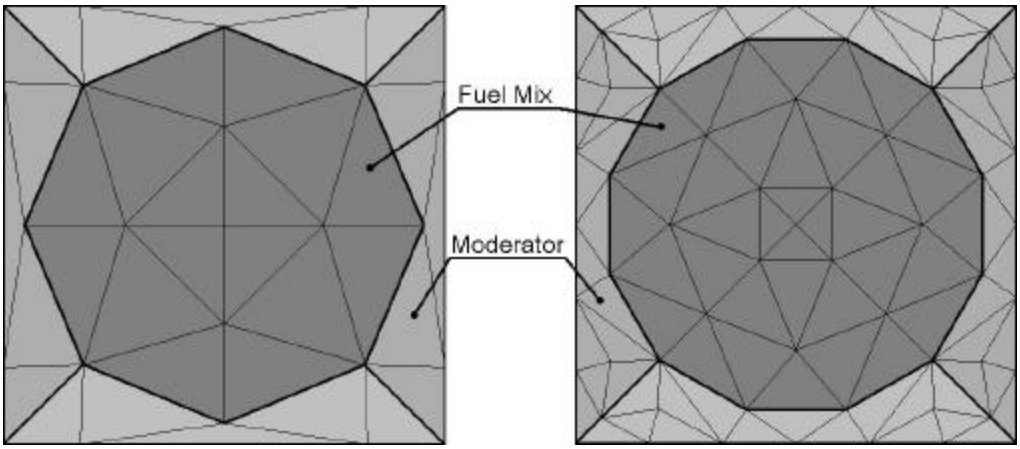

a. Course grid b. Fine grid.

Figure 1. Triangular Subelement Structures for a Fuel-pin Cell Sized Node

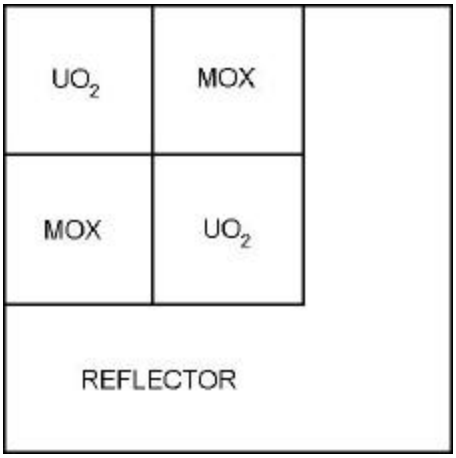

Figure. 2. Core Configuration for the C5 Benchmark Problem

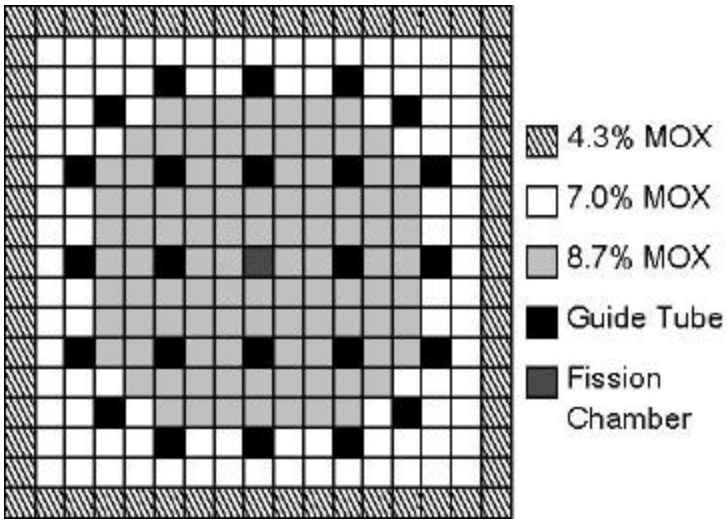

Figure 3. Composition Structure for a MOX Fuel Assembly

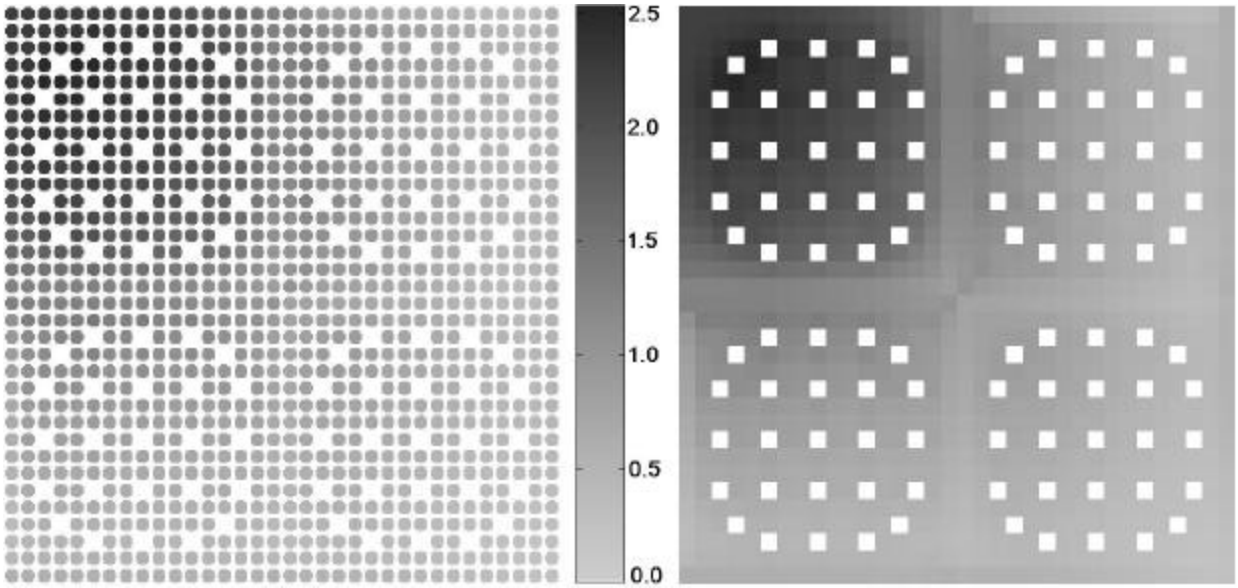

4a. **4b.**

Figure 4. a) Fuel Pin Powers for the C5 Problem without Homogenization
b) Fuel Pin Powers for the C5 Problem with Fuel-Pin Cell Homogenization